European Journal of Radiology 120 (2019) 108669

Contents lists available at ScienceDirect

European Journal of Radiology

journal homepage: www.elsevier.com/locate/ejrad

Histogram analysis parameters derived from DCE-MRI in head and neck squamous cell cancer – Associations with microvessel density

Hans-Jonas Meyer[a,*], Gordian Hamerla[a], Leonard Leifels[a], Anne Kathrin Höhn[b], Alexey Surov[a,c]

[a] Department of Diagnostic and Interventional Radiology, University of Leipzig, Leipzig, 04103, Germany
[b] Department of Pathology, University of Leipzig, Leipzig, Germany;c Department of Diagnostic and Interventional Radiology, Ulm University Medical Center, Albert-Einstein-Allee 23, 89081 Ulm, Germany;
[c] Department of Diagnostic and Interventional Radiology, Ulm University Medical Center, Albert-Einstein-Allee 23, 89081 Ulm, Germany

ARTICLE INFO

Keywords:
MRI
DCE MRI
HNSCC
MVD

ABSTRACT

Purpose: DCE MRI is a functional imaging modality, which is widely acknowledged to be linked to microvessel density in tissues. Therefore, it might be able to predict vessels in tumors. The present study sought to elucidate possible associations between microvessel density and histogram parameters in head and neck squamous cell carcinomas (HNSCC).

Method: 30 patients with histologically proven HNSCC were included in the study. DCE MRI was performed with a 3 T MRI and histogram analysis was calculated with a whole lesion measurement. In every case microvessel density was estimated with CD105 stained specimens.

Results: Median derived from K^{trans} correlated with vessel area ($\rho = 0.39$, $P = 0.034$). No other K_{trans} or V_e parameter reached statistically significance. Several K_{ep} derived parameters correlated with vessel area as well as with vessel count. MinK_{ep} had the highest correlation coefficient with vessel area ($\rho = 0.45$, $P = 0.01$). ModeK_{ep} had the highest coefficient with vessel count ($\rho = 0.41$, $P = 0.03$).

Conclusions: Histogram parameters derived from K_{ep} might be used as surrogate imaging biomarkers for microvessel density parameters in HNSCC. MinimumK_{ep} showed the highest correlation with vessel area and Mode K_{ep} with vessel count.

1. Introduction

Head and neck squamous cell carcinoma (HNSCC) is one of the most frequent malignancies [1]. The role of imaging in HNSCC is to locate the tumor, detect infiltration of the adjacent structures and to rule out possible metastasis [2]. However, modern functional imaging modalities, such as diffusion-weighted imaging (DWI) or dynamic-contrast enhanced MRI (DCE MRI), can provide further information regarding tumor microstructure [2]. According to the literature, DWI and DCE MRI can reflect several histopathological features like cellularity and microvessel density (MVD) and predict treatment success in different tumors [3–9]. For example, some preliminary reports showed that parameters of DCE MRI were associated with proliferation index Ki 67, cell count and microvessel area and vessel count in HNSCC [10–12].

DCE MRI is based on the serial acquisition of multiple T1-weighted images before, during and after intravenous injection of gadolinium based contrast agents [4] After the injection, the contrast medium diffuses from intravascular to the interstitial space, at a rate which is determined by the permeability of the capillary wall. The transfer of the contrast agent across the vessel wall can be quantified by applying a pharmacokinetic model. Typically, acquired parameters comprise volume transfer constant (K^{trans}), volume of the extravascular extracellular leakage space (V_e) and K_{ep}, reflecting diffusion of contrast medium from the extracellular space back to the plasma [13]. DCE MRI is widely acknowledged as a sensitive method for prediction of angiogenesis [14]. However, this might not be applied for every tumor entity [5]. For example, in a recent meta-analysis a wide range of correlation coefficients between K^{trans} and MVD was observed in different tumor entities [5]. Furthermore, it is still unclear, which DCE parameter might be best in prediction of MVD in tumors. So it was shown that V_e might reflect more aspects regarding cellularity and K^{trans} might be more important to reflect the amount of microvessels in tissues [11,15].

Nowadays, an emergent imaging analysis, namely histogram analysis, is used to further analyze radiological images. With this approach, every voxel of a ROI is issued into a histogram and, therefore, investigated tumors can be better characterized [16]. Presumably,

* Corresponding author.
E-mail address: Hans-Jonas.Meyer@medizin.uni-leipzig.de (H.-J. Meyer).

https://doi.org/10.1016/j.ejrad.2019.108669
Received 21 August 2018; Received in revised form 4 September 2019; Accepted 10 September 2019
0720-048X/ © 2019 Elsevier B.V. All rights reserved.

heterogeneity of the histogram might display heterogeneity of the tumor. The parameters, which can be calculated by using histogram analysis, are as follows: minimum, mean, maximum, median, mode, several percentiles, and second order statistics, namely kurtosis, skewness and entropy [16].

Previously, only few studies elucidated direct associations between MVD and DCE MRI in tumors [5]. So it might be crucial to better understand the relationships between imaging and histopathology. For example, DCE MRI parameters may be helpful to evaluate treatment response to antiangiogenesis therapy, which is known to alter strongly the structure and density of vessels in tumors.

Most studies investigating MVD derived from the antibodies CD31 and CD34, which stain all endothelial cells and, therefore, cannot distinguish between proliferating tumor vessels and physiological vessels [17]. Thus, CD105 or endoglin, can be used for selective staining of proliferating tumor vessels, which has been shown to be more related to patient outcome in HNSCC [17]. Previously, only one study directly compared the correlations between DCE MRI with CD31 and CD105 in breast cancer [18]. K^{trans} and K_{ep} strongly correlated with CD105 derived MVD but not with CD31 derived MVD [18]. This preliminary study might indicate that DCE MRI may reflect the proliferating tumor vessels better than the whole amount of vessels.

Therefore, in the present study CD105 stained specimen were used to elucidate possible associations between MVD and DCE MRI.

2. Materials and methods

This study was IRB-approved and all patients gave their written informed consent.

2.1. Patients

Overall, 30 patients (7 women and 23 men, mean age, 57.2 ± 10.8 years, median age, 56 years) with histologically proven HNSCC were included in the study. The diagnosed tumors were most often localized in the oropharynx (46.7% of the cases), tongue (23.3%), hypopharynx (10%), larynx (16.7%), and nasopharynx (3.3%). The identified lesions were staged as T1 and T2 in 26.7% of the cases, as T3 in 33.3% and as T4 tumors in 40%. Nodal metastases were found in 90%. In 36.7% the tumors were good and moderate differentiated and in 63.3% poorly differentiated.

2.1.1. Perfusion measurement

In all cases, DCE MRI was performed on a 3 T scanner (Siemens Biograph mMR; Siemens Healthcare, Erlangen, Germany) using a combined head and neck coil. T1w DCE sequences were used according to a protocol reported previously [17]. In brief, there were axial T1w vibe (volumetric interpolated breath-hold examination) DCE sequences with dual flip angle included 40 subsequent scans with a temporal resolution 6 s (40 slices per scan). Imaging parameters were as follows: TR/TE 4.14/2.46 ms, Field of view 260 mm, bandwidth 440 Hz/Px, slice thickness 4 mm, matrix 256 × 256, flip angles 2° and 8°, voxel size 1.2 × 1.0 × 4.0 mm, oversampling 27.3%. The total acquisition time was 4 min. No parallel imaging technique or under-sampling were used for the data acquisition. The contrast application (0.1 mmol Gadobutrol per kg of bodyweight, Gadovist®, Bayer Healthcare, Leverkusen, Germany) was started after the fifth scan at a rate of 3 ml per second and flushing with 10 ml of normal saline using a power injector (Spectris Solaris, Medrad, Bayer Healthcare, Leverkusen, Germany). The acquired images were transferred to a software module for tissue perfusion estimation (Tissue 4D, Siemens Medical Systems, Erlangen, Germany). The software offers a population based approach for the arterial input function (AIF) and the best of three available AIF-options was chosen according to the result of the chi2-parameter, which serves as an error measure for the model fit. The AIF was scaled in relation to the gadolinium dose and modeled according to the bi-exponential model of Tofts and Kermode [18].

The following pharmacokinetic parameters were calculated (for exemplary parameter images see Fig. 1A–E) [17,18]:

- K^{trans} (min^{-1}): volume transfer rate constant, which estimates the diffusion of contrast medium from the plasma through the vessel wall into the interstitial space, representing vessel permeability and blood flow;
- V_e (unitless): volume of the extravascular extracellular leakage space (EES);
- K_{ep} (min^{-1}): parameter for diffusion of contrast medium from the EES back to the plasma per unit volume tissue. It is in close relation with K_{trans} and V_e and is calculated by the formula $K_{ep} = K_{trans} \times V_e^{-1}$.

2.2. Histogram analysis

On the next step, the saved DICOM images were processed offline with custom-made Matlab-based application (The Mathworks, Natick, MA, USA). Thereafter, polygonal ROIs were manually drawn by one radiologist (AS, 16 years of radiological experience) on all of tumor displaying slides along the contours of the primary tumor in accordance to the t1-contrast enhancing tumor margin (whole lesion measure). The ROI was safely drawn within the tumor boundaries. For every perfusion parameter (K^{trans}, V_e, and K_{ep}) the following values were estimated: mean, maximal, minimal, and median values, as well percentiles 10th, 25th, 75th, and 90th. Furthermore, histogram-based characteristics, namely kurtosis, skewness, and entropy were calculated.

2.3. Histopathological analysis

In all cases the diagnosis of HNSCC was confirmed histopathologically by biopsy before any form of treatment. Representative tumor tissue slides from formalin-fixed paraffin-embedded tissue (bioptic specimens obtained in routinely work up) were processed after deparaffinization. The specimens were stained with CD105 antigen (Abcamplc, 330 Cambridge Science Park, Cambridge, CB4 0FL, UK). Overall, 2 high power fields (0.16 mm^2 per field) were selected for every tumor. All stained samples were digitalized by using a research microscope Jenalumar (Zeiss, Jena, Germany), with camera diagnostic instruments 4.2., magnification x400. Furthermore, the digital histopathological images were transferred as uncompressed TIFF images to ImageJ software (version 1.48v, NIH, Bethesda, MD) with a Windows system. MVD included the following parameters: stained vessel area (% per high power field), calculated as CD105 positive area divided by the total area of the analyzed histological specimens; total number of vessels according to Weidner et al (n) [19].

2.4. Statistical analysis

For statistical analysis the SPSS statistical software package was used (SPSS 20, SPSS Inc., Chicago IL, USA). Collected data were evaluated by means of descriptive statistics (absolute and relative frequencies). Categorical variables were expressed as percentages. P-values < 0.05 were taken to indicate statistical significance in all instances. After testing for normality distribution using Kolmogorov–Smirnov test, Spearman's correlation coefficient was used to analyze the associations between DCE MRI and MVD parameters.

3. Results

The descriptive statistics of the DCE MRI parameters including mean values and ranges are summarized in Table 1. Mean stained vessel area was 1.9% ± 1.11 with a range of 0.4–4.56 %. Mean vessel count was 11 with a SD of 4.56 and a range of 5–25 vessels per high power field.

Fig. 2 summarizes results of the correlation analysis in form of a

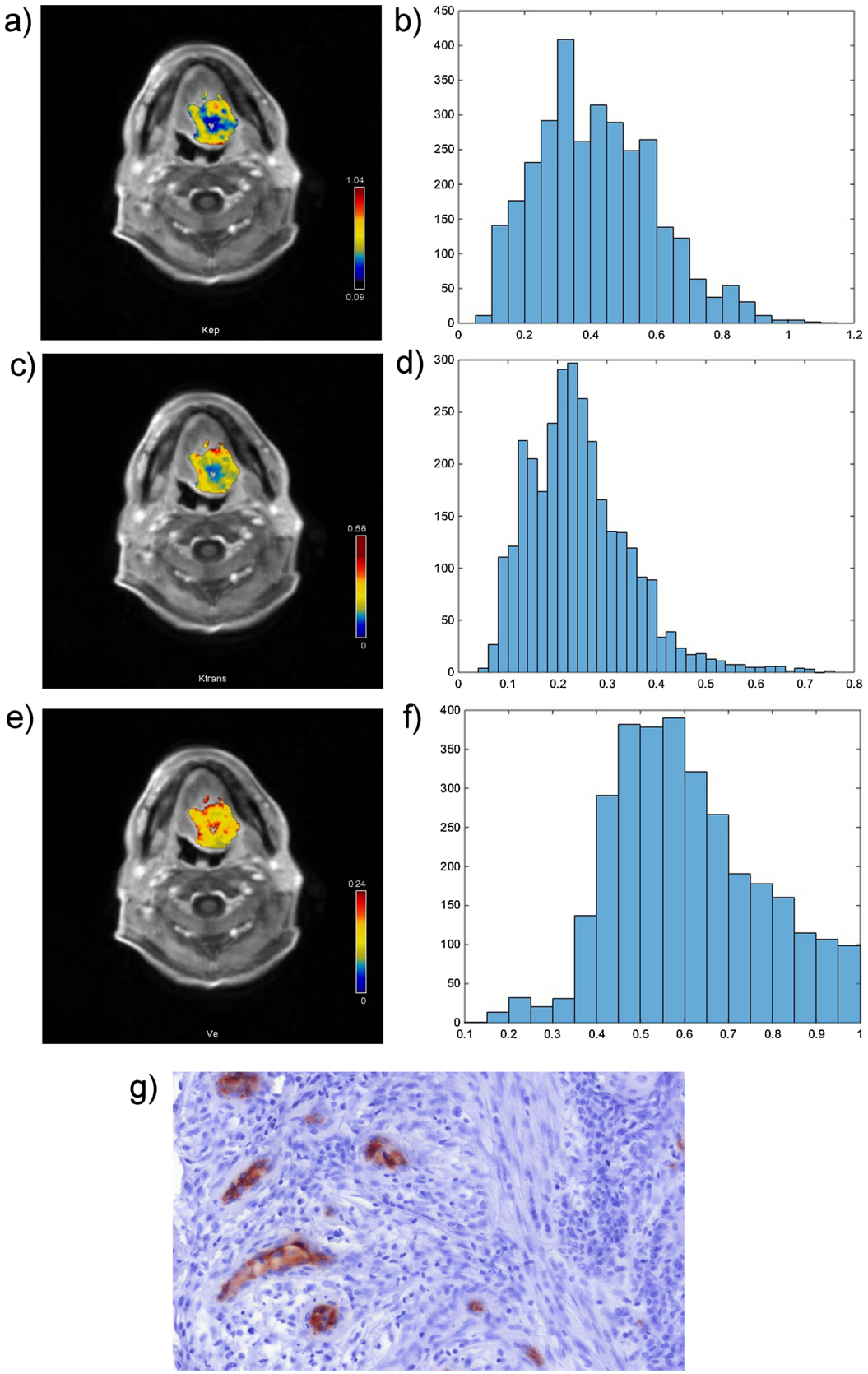

(caption on next page)

Fig. 1. Radiological and histopathological findings of a moderately differentiated (G2) oropharyngeal cancer (T4, N2, M0) in a 53 years old patient.
K_{ep}-map (a), K_{trans}-map (b) and of V_e-map (c) of a representative tumor slide. Histograms of the DCE MRI parameters using the whole lesion measurement (d, K_{ep}; e, K^{trans}; f, V_e). The histogram based parameters are as follows:
K_{ep} (min^{-1}): Mean 0.42, Min 0.08, Max 1.13, P10 0.19, P25 0.28, P75 0.54, P90 0.67, Median 0.4, Mode 0.4, Kurtosis 3.0, Skewness 0.55 and Entropy 3.81.
K^{trans} (min^{-1}): Mean 0.24, Min 0.06, Max 0.75, P10 0.12, P25 0.17, P75 0.30, P90 0.37, Median 0.23, Mode 0.20, Kurtosis K^{trans} 4.78, Skewness 1.00, and Entropy 4.27.
V_e (min^{-1}): Mean 0.61, Min 0.15, Max 1.0, P10 0.42, P25 0.48, P75 0.72, P90 0.85, Median 0.58, Mode 0.58, Kurtosis 2.66 Skewness 0.33, Entropy 3.70.
The CD105 stained specimen (g) showing a microvessel density of n = 8 according to Weidner et al. The stained vessel area is 2.64% of the high power field.

Table 1
a. Descriptive statistics of K^{trans}.

Parameter (min^{-1})	M ± SD	Range
Mean	0.19 ± 0.10	0.06–0.53
Min	0.05 ± 0.03	0.009–0.13
Max	0.61 ± 0.49	0.10–2.92
P10	0.11 ± 0.06	0.04–0.24
P25	0.14 ± 0.08	0.05–0.35
P75	0.24 ± 0.12	0.08–0.63
P90	0.30 ± 0.16	0.08–0.92
Median	0.18 ± 0.10	0.07–0.45
Mode	0.15 ± 0.09	0.04–0.47
Skewness	6.23 ± 6.29	2.68–33.70
Kurtosis	1.09 ± 0.81	−0.25–3.85
Entropy	3.30 ± 0.50	2.09–4.27

b. Descriptive statistics of K_{ep}.

Parameter (min^{-1})	M ± SD	Range
Mean	0.39 ± 0.16	0.15–0.89
Min	0.09 ± 0.06	0.01–0.22
Max	1.03 ± 0.56	0.31–2.97
P10	0.22 ± 0.11	0.07–0.58
P25	0.29 ± 0.13	0.10–0.72
P75	0.48 ± 0.19	0.19–1.04
P90	0.58 ± 0.22	0.23–1.19
Median	0.38 ± 0.16	0.15–0.89
Mode	0.35 ± 0.16	0.14–0.89
Skewness	4.70 ± 4.76	2.21–26.81
Kurtosis	0.64 ± 0.64	−0.25–2.52
Entropy	3.39 ± 0.55	2.20–4.38

c. Descriptive statistics of V_e.

Parameter (unitless)	M ± SD	Range
Mean	0.52 ± 0.17	0.16–0.79
Min	0.17 ± 0.10	0.03–0.36
Max	0.95 ± 0.14	0.44–0.99
P10	0.32 ± 0.15	0.09–0.58
P25	0.39 ± 0.17	0.12–0.70
P75	0.64 ± 0.20	0.19–0.92
P90	0.77 ± 0.20	0.25–0.97
Median	0.50 ± 0.19	0.15–0.83
Mode	0.43 ± 0.22	0.12–0.98
Skewness	3.03 ± 1.08	1.89-5.37
Kurtosis	0.43 ± 0.66	−1.41–1.55
Entropy	3.28 ± 0.60	1.55–4.12

heat map. Median derived from K^{trans} correlated with vessel area ($\rho = 0.39$, $P = 0.034$). No other K^{trans} or V_e parameter reached statistically significance. Several K_{ep} derived parameters correlated with vessel area as well as with vessel count. $MinK_{ep}$ had the highest correlation coefficient with vessel area ($\rho = 0.45$, $P = 0.01$). $ModeK_{ep}$ had the highest coefficient with vessel count ($\rho = 0.41$, $P = 0.03$) (Fig. 3).

4. Discussion

The present study identified associations between several DCE MRI parameters and MVD in HNSCC and provides relationships between imaging and histopathology. Furthermore, our results corroborated previous reported findings regarding the clinical role of DCE MRI in HNSCC.

Previously, some studies analyzed the possible benefit of DCE MRI in HNSCC [3,4,20]. So, it has been shown that DCE MRI might be able to differentiate between malignant and benign tumors [20,21]. Moreover, it can predict response to radiochemotherapy [4,22]. It can also provide prognostic information regarding overall survival in patients with HNSCC with nodal metastasis [23].

Presumably, DCE MRI may be associated with tissue microstructure characteristics in HNSCC based upon preliminary studies. In fact, it was shown that K_{ep} might reflect microvessel density features such as vessel area [11]. Moreover, V_e tended to correlate inversely with cellularity and K^{trans} with proliferation index (Ki 67) [11]. Furthermore, a strong positive correlation was found between the standard deviation derived from K_{ep} and VEGF expression, a very important angiogenesis related parameter [10].

The present study identified some significant associations between histogram parameters derived from DCE MRI and MVD. In contrast to the abovementioned previous studies, which used a conventional imaging analysis, we used a whole lesion histogram analysis derived from DCE MRI. We hypothesized that this approach might identify more associations with MVD than previously analyzed parameters because the whole tumor can be assessed. In fact, we observed several significant correlations between the investigated findings. For example, $MinK_{ep}$ had the highest correlation coefficient with vessel area. This parameter represents the voxel with the lowest value within the tumor. For ADC values derived from diffusion-weighted imaging it is known that the minimum value displays the tumor area with the highest cellularity and, therefore, presumably, the area with the highest malignant potential [24,25]. Regarding DCE MRI such an association was not published previously. This finding may suggest that $MinK_{ep}$ might be a potential imaging biomarker for prediction of MVD in HNSCC.

Furthermore, according to the literature, K_{ep} may also predict other histopathological features. So, it was correlated with matrix metalloproteinase 9 expression in glioblastoma [26]. Moreover, K_{ep} had the highest correlations with FDG-PET parameters in HNSCC [27]. This finding suggests that K_{ep} might represent a parameter, which reflects a complex interaction between perfusion and metabolic activity.

K_{ep} determines the washout rate from the extracellular and extravascular space back into the blood plasma [20]. Our data suggest that this might be more related to the amount of proliferating tumor vessels than the initial extravasation of contrast media, reflected by K^{trans}. The exact reasons for this finding are unclear.

Furthermore, the present study showed that histogram analysis can better characterize tumors than the conventional single ROI based approach. Using the whole lesion histogram analysis, crucial information of the whole tumor can be analyzed and data about statistical distribution of obtained values can be provided. It is widely believed that heterogeneity of the histogram might also be able to predict heterogeneity of the microstructure in histopathology specimen [16].

As shown, none of the V_e related parameter correlated with MVD. This is in good agreement with the published data [10,11]. V_e might be able to reflect extracellular spaces in tissues and, thus, might inversely correlate with cellularity. This was shown in a glioma mouse model. The calculated correlation coefficient between V_e and cell count was -0.75 [15]. Similar results were also reported in HNSCC [12]. This is corroborated by the reported finding that V_e correlated well with ADC

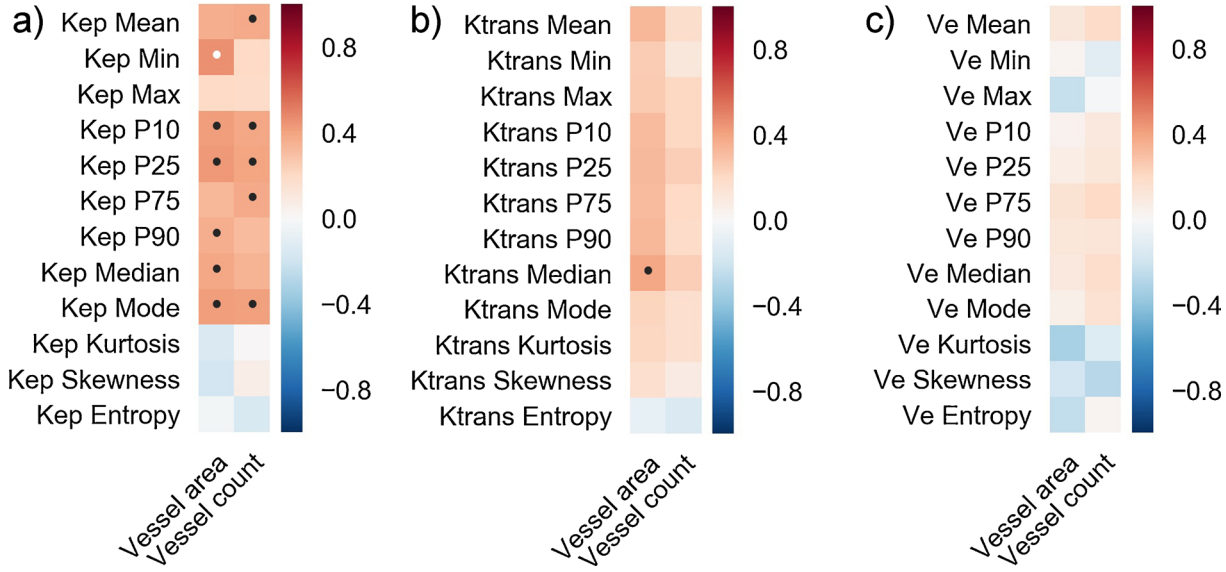

Fig. 2. Heat maps displaying the Spearman correlation analysis in a color coded fashion.
a. Correlations between histogram parameters derived from K_{ep} and microvessel density. MinK_{ep} correlates statistically significant with vessel area ($\rho = 0.45$, $P = 0.01$) (displayed by the white dot). Other statistically significant correlations are depicted by black dots.
b. Correlations between histogram parameters derived from K^{trans} and microvessel density. Only Median correlates statistically significant with vessel area ($\rho = 0.39$, $P = 0.034$) (displayed by the black dot).
c. Correlations between histogram parameters derived from V_e and microvessel density. There are no statistically significant correlations.

values in HNSCC [28]. ADC values are widely acknowledged to be inversely correlated with cellularity in tumors [8,24].

Furthermore, in the present study, median derived from K^{trans} correlated with vessel area. Previous reports did not find significant correlations between K^{trans} and MVD [10,11]. This phenomenon may be related to the fact that histogram analysis parameters may be more sensitive than mean values used in the previous investigations.

In summary, the present study indicated that different parameters derived from DCE MRI are able to reflect different tumor aspects in HNSCC. K_{ep} seems to be more sensitive for microvessel density, V_e for cellularity and K^{trans} for proliferation potential. Clearly, further studies are needed to confirm these assumptions.

It is of note that MVD measurement is a quantitative morphological index and might not reflect every functional aspect of tissue microvasculature, including permeability which contributes to the DCE MRI measurement [29]. Some stained vessel might be non-functional and thus there might be a statistical error between the sole amount of vessel and the functional imaging modality.

Important, in the present study MVD was measured based on CD105 expression. As mentioned above, previously, most studies analyzed MVD parameters on CD31 or CD34 stained specimens and only few reports performed similar analysis as in our study [30,31]. It is well known that the degree of microvascular stimulation resulting from angiogenesis. CD105 is associated with new and immature microvessels [30–33]. Therefore, CD105 may be a biomarker for novel angiogenic microvessels [34]. CD105 positive microvessels are immature and increase permeability [30,31]. Furthermore, the increased permeability of CD105-positive microvessels can cause vascular contents to leak into the extravascular space [35].

Therefore, MVD parameters retrieved from CD105 staining identify only tumor-related vasculature and, therefore, may play a greater role in clinical practice than other staining methods. In fact, it has been shown that CD105 specific expression in astrocytoma microvascular endothelial cells and CD105-MVD of different glioma grades increased as pathologic grade gradually increased [6,10]. According to Jia et al., CD105-MVD of low grade gliomas was significantly lower than that of high grade tumors [30].

Some previous studies indicated that DCE MRI parameters may predict treatment success and clinical outcome in HNSCC. For example, Ng et al. showed that Kep of primary tumour, Ve of lymph node metastases and SUVmax of primary tumour were independent prognosticators for oropharyngeal or hypopharyngeal squamous cell carcinomas treated with chemoradiation [36]. Similarly, Yoo et al mentioned that pretreatment and early DCE MRI may identify patients at possible risk of treatment failure [37]. Our study identified links between histopathology, in particular MVD, and DCE MRI and may explain the possibility of DCE MRI to predict follow up in patients with HNSCC.

There are several limitations of the present study to address. Firstly, the patient sample is rather small, but larger than in two comparable preliminary studies published before [10,11]. Secondly, the histopathology analysis was performed on bioptic specimen, which might not be fully representative of the whole tumor, whereas the MRI analysis was performed as a whole lesion measurement. This might result in some incongruities. Thirdly, histogram analysis is influenced by several factors. So it was shown that the ROI method has a substantial influence on the reproducibility of histogram parameters [38]. However, the whole lesion measurement, as it was performed in the present study, showed a higher reproducibility than a single slide approach [38]. Furthermore, parameters, like skewness, kurtosis, entropy might have a lower reproducibility [39]. Fourthly, DCE MRI in the head and neck region is challenging because of susceptibility to metal artifacts and motion from swallowing and breathing, which might have an influence on the histogram parameters.

In the present study, whole tumor measure was performed for estimation of DCE MRI parameters. Notably, some authors indicated that tumoral perfusion heterogeneity should be addressed for such analyses. In fact, Giesel et al. selected ROIs for subanalysis of DCE MRI maps, particularly for search of highly vascular regions or “hot spots” within the tumor [40]. The authors mentioned that this analysis can reflect the status of different populations of angiogenic vessels i.e. highly vascular and permeable and highly vascular but moderately permeable [40].

Furthermore, we did not analyze heterogeneity of MVD in the estimated tumors. As reported by van Niekerk et al., MVD is very heterogeneous and characteristics of tumour vascularity depend on those in normal surrounding tissue [41]. Therefore, it is recommended to

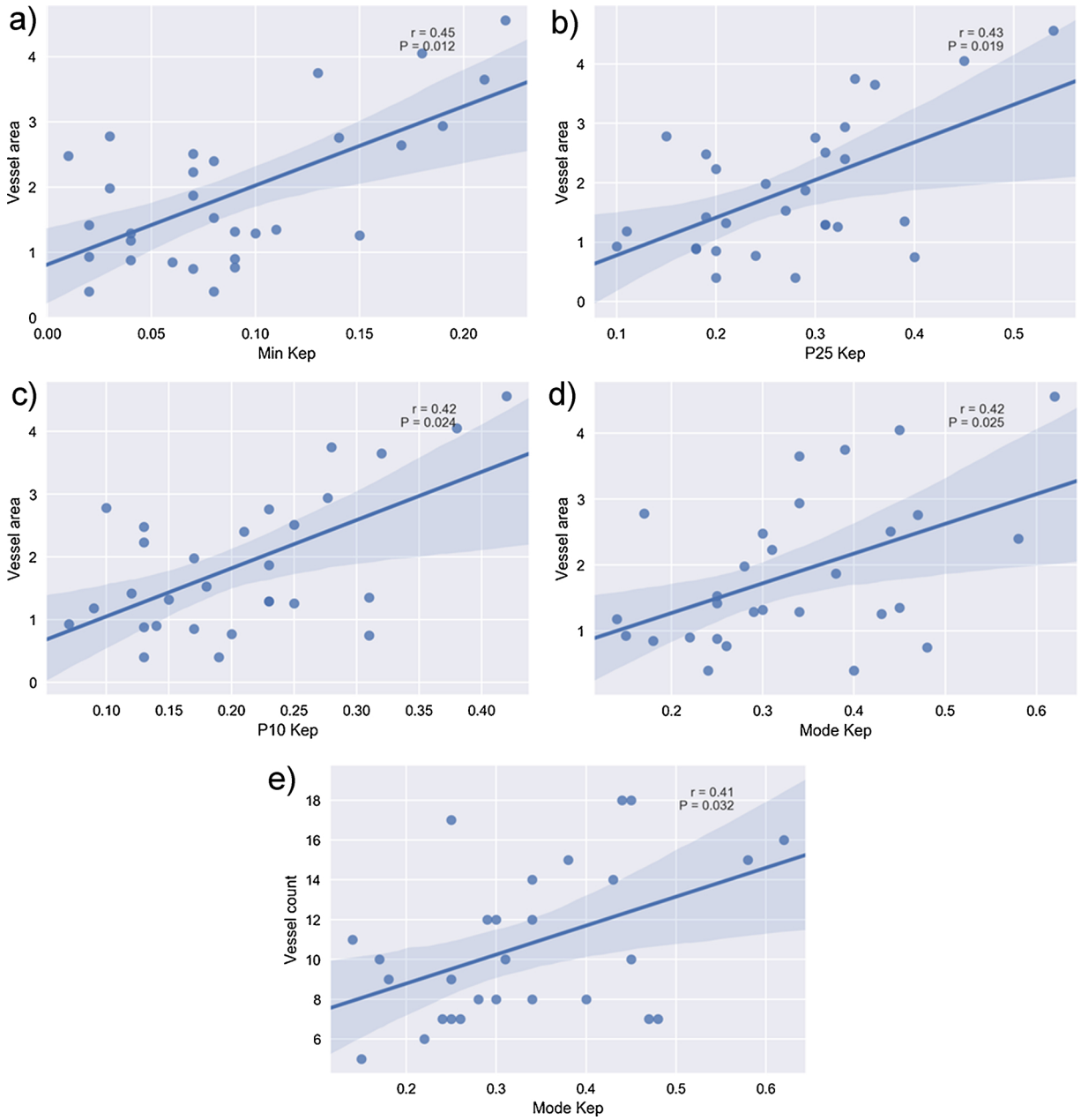

Fig. 3. Graphs of the statistically significant correlations.
a. Correlation between MinK_{ep} and vessel area (r = 0.45, P = 0.012), the unit of K_{ep} is min^{-1} and for vessel area it is % of the high power field.
b. Correlation between P25K_{ep} and vessel area (r = 0.42, P = 0.024), the unit of K_{ep} is min^{-1} and for vessel area it is % of the high power field.
c. Correlation between P10K_{ep} and vessel area (r = 0.42, P = 0.012), the unit of K_{ep} is min^{-1} and for vessel area it is % of the high power field.
d. Correlation between ModeK_{ep} and vessel area (r = 0.42, P = 0.025), the unit of K_{ep} is min^{-1} and for vessel area it is % of the high power field.
e. Correlation between ModeK_{ep} and vessel count (r = 0.41, P = 0.032), the unit of K_{ep} is min^{-1} and for vessel area it is % of the high power field.

calculate a ratio between tumoral and normal tissue vascularity parameters to amend individual microvascularity variations [41].

Finally, in our study we used the perfusion model according to Toft and Kernel [19]. This model does not include some important perfusion parameters like vascular volume fraction. According to the literature, vascular volume fraction is probably the most relevant parameter to reflect MVD [42–44]. For example, Consolino et al. analyzed associations between DCE MRI and MVD in gastrointestinal stromal tumors and observed strong correlations between MVD and vascular volume fraction [42]. Furthermore, vascular volume fraction also correlated well with permeability measured by mean dextran density [42].

Clearly, relationships between DCE MRI and histopathology may be more complex than it is shown is the present study. Further studies are needed to investigate associations between other DCE MRI parameters and histopathological features in several malignant diseases.

5. Conclusion

The present study showed that histogram parameters derived from K_{ep} might be used as surrogate imaging biomarkers for microvessel density parameters in HNSCC. MinimumK_{ep} showed the highest correlation with vessel area and Mode K_{ep} with vessel count.

Funding

None

Declaration of Competing Interest

The authors declare no conflict of interest.

References

[1] D.C. Beachler, A.G. Abraham, M.J. Silverberg, Y. Jing, C. Fakhry, M.J. Gill, R. Dubrow, M.M. Kitahata, M.B. Klein, A.N. Burchell, P.T. Korthuis, R.D. Moore, G. D'Souza, Incidence and risk factors of HPV-related and HPV-unrelated head and neck squamous cell carcinoma in HIV-infected individuals, Oral Oncol. 50 (2014) 1169–1176.

[2] G. Widmann, B. Henninger, C. Kremser, W. Jaschke, MRI sequences in head & neck radiology - state of the art, Rofo. 189 (2017) 413–422.

[3] D.P. Noij, M.C. de Jong, L.G. Mulders, J.T. Marcus, R. de Bree, C. Lavini, P. de Graaf, J.A. Castelijns, Contrast-enhanced perfusion magnetic resonance imaging for head and neck squamous cell carcinoma: a systematic review, Oral Oncol. 51 (2015) 124–138.

[4] J.M. Bernstein, J.J. Homer, C.M. West, Dynamic contrast-enhanced magnetic resonance imaging biomarkers in head and neck cancer: potential to guide treatment? A systematic review, Oral Oncol. 50 (2014) 963–970.

[5] H.J. Meyer, A. Wienke, A. Surov, Correlation between k_{trans} and microvessel density in different tumors: a meta-analysis, Anticancer Res. 38 (2018) 2945–2950.

[6] R. Sinkus, B.E. Van Beers, V. Vilgrain, N. DeSouza, J.C. Waterton, Apparent diffusion coefficient from magnetic resonance imaging as a biomarker in oncology drug development, Eur. J. Cancer 48 (2012) 425–431.

[7] A.R. Padhani, G. Liu, D.M. Koh, T.L. Chenevert, H.C. Thoeny, T. Takahara, A. Dzik-Jurasz, B.D. Ross, M. Van Cauteren, D. Collins, D.A. Hammoud, G.J. Rustin, B. Taouli, P.L. Choyke, Diffusion-weighted magnetic resonance imaging as a cancer biomarker: consensus and recommendations, Neoplasia 11 (2009) 102–125.

[8] A. Surov, H.J. Meyer, A. Wienke, Correlation between apparent diffusion coefficient (ADC) and cellularity is different in several tumors: a meta-analysis, Oncotarget 8 (2017) 59492–59499.

[9] A. Surov, H.J. Meyer, A. Wienke, Associations between apparent diffusion coefficient (ADC) and KI 67 in different tumors: a meta-analysis. Part 1: ADC_{mean}, Oncotarget 8 (2017) 75434–75444.

[10] J.F. Jansen, D.L. Carlson, Y. Lu, H.E. Stambuk, A.L. Moreira, B. Singh, S.G. Patel, D.H. Kraus, R.J. Wong, A.R. Shaha, J.P. Shah, A. Shukla-Dave, Correlation of a priori DCE-MRI and (1)H-MRS data with molecular markers in neck nodal metastases: initial analysis, Oral Oncol. 48 (2012) 717–722.

[11] A. Surov, H.J. Meyer, M. Gawlitza, A.K. Höhn, A. Boehm, T. Kahn, P. Stumpp, Correlations between DCE MRI and histopathological parameters in head and neck squamous cell carcinoma, Transl. Oncol. 10 (2017) 17–21.

[12] A. Surov, H.J. Meyer, L. Leifels, A.K. Höhn, C. Richter, K. Winter, Histogram analysis parameters of dynamic contrast-enhanced magnetic resonance imaging can predict histopathological findings including proliferation potential, cellularity, and nucleic areas in head and neck squamous cell carcinoma, Oncotarget 9 (2018) 21070–21077.

[13] F. Khalifa, A. Soliman, A. El-Baz, M. Abou El-Ghar, T. El-Diasty, G. Gimel'farb, R. Ouseph, A.C. Dwyer, Models and methods for analyzing DCE-MRI: a review, Med. Phys. 41 (2014) 124301.

[14] H. Li, L. Yu, W. Wang, L. Wang, X. Zheng, S. Dai, Y. Sun, Dynamics of angiogenesis and cellularity in rabbit VX2 tumors using contrast-enhanced magnetic resonance imaging and diffusion-weighted imaging, Oncol. Lett. 15 (2018) 2978–2984.

[15] M.P. Aryal, T.N. Nagaraja, K.A. Keenan, H. Bagher-Ebadian, S. Panda, S.L. Brown, G. Cabral, J.D. Fenstermacher, J.R. Ewing, Dynamic contrast enhanced MRI parameters and tumor cellularity in a rat model of cerebral glioma at 7 T, Magn. Reson. Med. 71 (2014) 2206–2214.

[16] N. Just, Improving tumour heterogeneity MRI assessment with histograms, Br. J. Cancer 111 (2014) 2205–2213.

[17] T. Martone, P. Rosso, R. Albera, G. Migliaretti, F. Fraire, L. Pignataro, G. Pruneri, G. Bellone, G. Cortesina, Prognostic relevance of CD105+ microvessel density in HNSCC patient outcome, Oral Oncol. 41 (2005) 147–155.

[18] L. Li, K. Wang, X. Sun, K. Wang, Y. Sun, G. Zhang, B. Shen, Parameters of dynamic contrast-enhanced MRI as imaging markers for angiogenesis and proliferation in human breast cancer, Med. Sci. Monit. 21 (2015) 376–382.

[19] P.S. Tofts, A.G. Kermode, Measurement of the blood–brain barrier permeability and leakage space using dynamic MR imaging. 1. Fundamental concepts, Magn. Reson. Med. 17 (1991) 357–367.

[20] N. Weidner, J.P. Semple, W.R. Welch, J. Folkman, Tumor angiogenesis and metastasis–correlation in invasive breast carcinoma, N. Engl. J. Med. 324 (1991) 1–8.

[21] S. Marzi, F. Piludu, C. Forina, G. Sanguineti, R. Covello, G. Spriano, A. Vidiri, Correlation study between intravoxel incoherent motion MRI and dynamic contrast-enhanced MRI in head and neck squamous cell carcinoma: evaluation in primary tumors and metastatic nodes, Magn. Reson. Imaging 37 (2017) 1–8.

[22] A.A. Razek, L.G. Elsorogy, N.Y. Soliman, N. Nada, Dynamic susceptibility contrast perfusion MR imaging in distinguishing malignant from benign head and neck tumors: a pilot study, Eur. J. Radiol. 77 (2011) 73–79.

[23] P.J. Hoskin, M.I. Saunders, K. Goodchild, M.E. Powell, N.J. Taylor, H. Baddeley, Dynamic contrast enhanced magnetic resonance scanning as a predictor of response to accelerated radiotherapy for advanced head and neck cancer, Br. J. Radiol. 72 (1999) 1093–1098.

[24] A. Shukla-Dave, N.Y. Lee, J.F. Jansen, H.T. Thaler, H.E. Stambuk, M.G. Fury, S.G. Patel, A.L. Moreira, E. Sherman, S. Karimi, Y. Wang, D. Kraus, J.P. Shah, D.G. Pfister, J.A. Koutcher, Dynamic contrast-enhanced magnetic resonance imaging as a predictor of outcome in head-and-neck squamous cell carcinoma patients with nodal metastases, Int. J. Radiat. Oncol. Biol. Phys. 82 (2012) 1837–1844.

[25] A. Surov, H.J. Meyer, A. Wienke, Correlation between minimum apparent diffusion coefficient (ADC_{min}) and tumor cellularity: a meta-analysis, Anticancer Res. 37 (2017) 3807–3810.

[26] R. Awasthi, C.M. Pandey, P. Sahoo, S. Behari, V. Kumar, S. Kumar, S. Misra, N. Husain, P. Soni, R.K. Rathore, R.K. Gupta, Dynamic contrast-enhanced magnetic resonance imaging-derived kep as a potential biomarker of matrix metalloproteinase 9 expression in patients with glioblastoma multiforme: a pilot study, J. Comput. Assist. Tomogr. 36 (2012) 125–130.

[27] A. Surov, L. Leifels, H.J. Meyer, K. Winter, O. Sabri, S. Purz, Associations Between Histogram Analysis DCE MRI Parameters and Complex $_{18}$F-FDG-PET Values in Head and Neck Squamous Cell Carcinoma, Anticancer Res. 38 (2018) 1637–1642.

[28] H.J. Meyer, L. Leifels, S. Schob, N. Garnov, A. Surov, Histogram analysis parameters identify multiple associations between DWI and DCE MRI in head and neck squamous cell carcinoma, Magn. Reson. Imaging 45 (2018) 72–77.

[29] N. Hylton, Dynamic contrast-enhanced magnetic resonance imaging as an imaging biomarker, J. Clin. Oncol. 24 (2006) 3293–3298.

[30] Z.Z. Jia, H.M. Gu, X.J. Zhou, J.L. Shi, M.D. Li, G.F. Zhou, X.H. Wu, The assessment of immature microvascular density in brain gliomas with dynamic contrast-enhanced magnetic resonance imaging, Eur. J. Radiol. 84 (2015) 1805–1809.

[31] Z.Z. Jia, W. Shi, J.L. Shi, D.D. Shen, H.M. Gu, X.J. Zhou, Comparison between perfusion computed tomography and dynamic contrast-enhanced magnetic resonance imaging in assessing glioblastoma microvasculature, Eur. J. Radiol. 87 (2017) 120–124.

[32] H.B. Salvesen, M.G. Gulluoglu, I. Stefansson, L.A. Akslen, Significance of CD 105 expression for tumour angiogenesis and prognosis in endometrial carcinomas, APMIS. 111 (2003) 1011–1018.

[33] P. Kumar, J.M. Wang, C. Bernabeu, CD 105 andangiogenesis, J. Pathol. 178 (1996) 363–366.

[34] S. Behrem, K. Zarkovic, N. Eskinja, N. Jonjic, Endoglin is a better marker than CD31 in evaluation of angiogenesis in glioblastoma, Croat. Med. J. 46 (2005) 417–422.

[35] S.J. Smith, H. Tilly, J.H. Ward, D.C. Macarthur, J. Lowe, B. Coyle, R.G. Grundy, CD105 (Endoglin) exerts prognostic effects via its role in the microvascular niche of paediatric high grade glioma, Acta Neuropathol. 124 (2012) 99–110.

[36] S.H. Ng, C.T. Liao, C.Y. Lin, S.C. Chan, Y.C. Lin, T.C. Yen, J.T. Chang, S.F. Ko, K.H. Fan, H.M. Wang, L.Y. Yang, J.J. Wang, Dynamic contrast-enhanced MRI, diffusion-weighted MRI and ^{18}F-FDG PET/CT for the prediction of survival in oropharyngeal or hypopharyngeal squamous cell carcinoma treated with chemoradiation, Eur. Radiol. 26 (2016) 4162–4172.

[37] D.S. Yoo, J.P. Kirkpatrick, O. Craciunescu, G. Broadwater, B.L. Peterson, M.D. Carroll, R. Clough, J.R. MacFall, J. Hoang, R.L. Scher, R.M. Esclamado, F.R. Dunphy, N.E. Ready, D.M. Brizel, Prospective trial of synchronous bevacizumab, erlotinib, and concurrent chemoradiation in locally advanced head and neck cancer, Clin. Cancer Res. 18 (2012) 1404–1414.

[38] J.L. Ren, Y. Yuan, X.X. Li, Y.Q. Shi, X.F. Tao, Histogram analysis of apparent diffusion coefficient maps in the prognosis of patients with locally advanced head and neck squamous cell carcinoma: comparison of different region of interest selection methods, Eur. J. Radiol. 106 (2018) 7–13.

[39] H.Y. Wang, Z.H. Su, X. Xu, Z.P. Sun, F.X. Duan, Y.Y. Song, L. Li, Y.W. Wang, X. Ma, A.T. Guo, L. Ma, H.Y. Ye, Dynamic contrast-enhanced MR imaging in renal cell carcinoma: reproducibility of histogram analysis on pharmacokinetic parameters, Sci. Rep. 6 (2016) 29146.

[40] F.L. Giesel, P.L. Choyke, A. Mehndiratta, C.M. Zechmann, H. von Tengg-Kobligk, K. Kayser, H. Bischoff, C. Hintze, S. Delorme, M.A. Weber, M. Essig, H.U. Kauczor, M.V. Knopp, Pharmacokinetic analysis of malignant pleural mesothelioma-initial results of tumor microcirculation and its correlation to microvessel density (CD-34), Acad. Radiol. 15 (2008) 563–570.

[41] C.G. van Niekerk, J.A. van der Laak, T. Hambrock, H.J. Huisman, J.A. Witjes, J.O. Barentsz, C.A. Hulsbergen-van de Kaa, Correlation between dynamic contrast-enhanced MRI and quantitative histopathologic microvascular parameters in organ-confined prostate cancer, Eur. Radiol. 24 (2014) 2597–2605.

[42] L. Consolino, D.L. Longo, M. Sciortino, W. Dastrù, S. Cabodi, G.B. Giovenzana, S. Aime, Assessing tumor vascularization as a potential biomarker of imatinib resistance in gastrointestinal stromal tumors by dynamic contrast-enhanced magnetic resonance imaging, Gastric Cancer 20 (2017) 629–639.

[43] L. Consolino, D.L. Longo, W. Dastrù, J.C. Cutrin, D. Dettori, S. Lanzardo, S. Oliviero, F. Cavallo, S. Aime, Functional imaging of the angiogenic switch in a transgenic mouse model of human breast cancer by dynamic contrast enhanced magnetic resonance imaging, Int. J. Cancer 139 (2016) 404–413.

[44] J.R. Ewing, H. Bagher-Ebadian, Model selection in measures of vascular parameters using dynamic contrast-enhanced MRI: experimental and clinical applications, NMR Biomed. 26 (2013) 1028–1041.